Characterization of IGBTs Short-Circuit Fault in an Arm Configuration Considering Devices Intrinsic Discrepancies

N. Mohammad-Bagheri Bafghi[1], S. Mohsenzade[2*], *Member, IEEE*

[1] Department of Electrical Engineering, K. N. Toosi University of Technology, Tehran, Iran, (ORCID:0009-0008-3087-3327), n.mohammadbagheribafghi@email.kntu.ac.ir
[2] Department of Electrical Engineering, K. N. Toosi University of Technology, Tehran, Iran, (ORCID:0000-0003-0206-8570), s.mohsenzade@kntu.ac.ir

***Abstract*—The short circuit fault (SCF) is a dangerous condition threatening the health of insulated gate bipolar transistors (IGBTs). Thus, SCF can be considered a critical issue for the reliability of power electronic converters. The SCF behavior of IGBTs and their failure factors when operating in an arm configuration are the focus of this paper. This paper considers the non-idealities of the circuit and differences in IGBT parameters and describes the SCF fault. It was found that there is a significant voltage imbalance among the IGBTs during SCF, which leads to a notable energy imbalance between the devices. The voltage and energy imbalances depend significantly on the inevitable discrepancies in the circuitry and internal parameters of the IGBTs. To verify these findings, a detailed PSPICE simulation is conducted, and experimental results are also reported for different scenarios in SCFs. The results confirm that short-circuit energy among the devices can differ significantly. Moreover, the voltage distribution across IGBTs strongly depends on both their intrinsic parameter mismatches and the operating conditions.**

***Index Terms*—Reliability, IGBT, Overvoltage protection, Short circuit fault.**

I. INTRODUCTION

As the use of power electronics converters expands in various domains such as power transmission, renewable energy systems, adjustable-speed drives, electric vehicles, etc., it becomes imperative to examine system reliability and assess operational risks [1]. Accordingly, the reliability of industrial power converters is a critical issue due to the use of vulnerable components, such as high-power semiconductor switches and capacitors [2]. These components (switches and capacitors) are responsible for about 34% of unexpected interruptions [3]-[5]. The failure of a component in the power electronics converter may cause the entire system to shut down [6], [7]. These unpredictable shutdowns, in addition to safety hazards, result in higher operational costs [8]-[11]. The reliability of power converters can be investigated from two different perspectives: fault management, which deals with the detection, protection, and handling of abrupt and critical failures such as short or open circuits, and lifetime management, which focuses on the aging and degradation processes of components over time. Fault management usually relies on circuit breakers and fault characterization to protect the converter and ensure correct system behavior [12], whereas lifetime management emphasizes reliability prediction and lifetime extension by addressing aging mechanisms [13], [14].

Insulated Gate Bipolar Transistors (IGBTs) are among the most important power semiconductor switches in medium- and high-power converters [15] because of their low on-state loss, voltage-controlled operation, and short-circuit fault (SCF) withstand capability [16], [17]. The ability of IGBTs to endure SCF for a limited time (about 10 µs) over 10,000 times (if the SCF energy is below the critical energy, $E_{SCF} < E_{Critical}$) is very appealing [18]. This feature makes IGBTs suitable for applications prone to short-circuit faults. However, while IGBTs can tolerate SCF energy, they are highly vulnerable to overvoltages during and post-fault situations. Overvoltage conditions for IGBTs are very common when they are used in series structures and are deeply investigated in [16], [19], and [20]. The dangerous overvoltage condition for IGBTs in series structures arises due to differences in their intrinsic parameters during SCF. To address this critical issue and alleviate the overvoltage stress on IGBTs, different types of snubbers have been proposed in [14] and [20].

The arm configuration (Figure 1) is a common circuit in the aforementioned applications. It can be found in PV inverters, motor drives, single- and three-phase inverters, and DC/DC converters such as full- and half-bridge topologies [21], [22], or as submodules in modular multilevel converters (MMCs) [23]. Several studies have been conducted on the characterization of single IGBT SCF [24]-[28], series-connected IGBTs [16], [29], parallel-connected IGBTs [30], and IGBTs connected in bridge structures [31]. In these articles (except [31]), gate-drive circuits are assumed to work ideally, and intrinsic failures cause SCF. However, as a common malfunction, SCF may occur when an incorrect gate signal is applied to the high-side or low-side of the arm configuration. Driver circuit malfunctions, failures in the auxiliary power supply, dv/dt disturbances [32], or shoot-through cross-talk [33], [34] can result in incorrect gate signals. There are few studies describing IGBT short-circuit behavior in an arm configuration. In this specific case, the IGBTs are connected in series structures but carry different levels of SCF currents. As a result, serious voltage and energy imbalances occur, which can be fatal for IGBTs. In [31], the behavior of SCF in an arm

configuration is discussed, and an equation for voltage distribution is established. However, in [31], the IGBTs in the arm configuration are assumed to be completely identical, which is not very probable in real applications. Even IGBTs with the same part number may have intrinsic differences [16].

This paper aims to characterize IGBTs' SCF behavior in an arm configuration, considering intrinsic parameter discrepancies. This investigation focuses on inequalities in parameters such as transconductance, threshold voltage, and gate-emitter voltage. Based on the achievements of this paper, the inequalities in device parameters result in different voltage and energy distributions across IGBTs, which differ from the findings of prior works.

The main contributions of this paper regarding the SCF behavior of IGBTs in an arm configuration are as follows:

- There is a considerable voltage and energy imbalance between two IGBTs in an arm configuration during SCF.
- The voltage redistribution is not decisive in all conditions, which modifies the conclusions of [31].
- The voltage and energy distributions across IGBTs depend on both intrinsic parameters and circuit-related factors.

The rest of the paper is organized as follows. Section II presents the single IGBT behavior in the case of a short-circuit event and then analyzes the dependence of IGBT short-circuit behavior on intrinsic parameters. Section III presents the behavior of the IGBT SCF in an arm structure, considering either identical or non-identical IGBTs. By simulations in Section IV, the impacts of switch mismatches on voltage distributions will be demonstrated. Section V has the test prototype and experimental results.

II. SINGLE IGBT SCF BEHAVIOR

The transfer characteristic of an IGBT is divided into two regions: the Active and Saturation regions (as shown in Figure 2). During SCF, the IGBT operates in active region of its transfer characteristics. In this condition, the short-circuit current is limited by the physical structure of the IGBT. Using the steady-state model of the IGBT in Active region, Saturation collector current during SCF is given in [16], [35]:

$$I_C = (1+\beta_{PNP})\frac{\mu_{ni}C_{ox}Z}{2L_{CH}}(V_{GE}-V_{th})^2 + \frac{V_{CE}}{R_o} \qquad (1)$$

$$g_{fs} = \frac{dI_C}{dV_{GE}} = (1+\beta_{PNP})\frac{\mu_{ni}C_{ox}Z}{L_{CH}}(V_{GE}-V_{th});$$

$$I_C = g_{fs}(V_{GE}-V_{th}) + \frac{V_{CE}}{R_o}$$

where β_{PNP} denotes the common-emitter gain of the PNP transistor, μ_{ni} is the average electron mobility in the channel, C_{ox} is oxide capacitance per unit area, Z is the channel width, L_{CH} is the channel length, g_{fs} represents the transconductance, V_{GE} is the gate-emitter voltage, V_{th} is the gate-emitter threshold voltage, V_{CE} is the collector- emmiter voltage and R_o is the output resistance of the IGBT.

The non-linear gate-emitter voltage characteristics lead to a threshold voltage that differs from datasheet specifications under short-circuit conditions. To utilize equation (1), Linearization of collector current–gate-emitter voltage characteristic is required (Figure 3). A modified version of equation (1) is presented to accommodate this non-linearity:

$$I_C = g_{fs}(V_{GE}-V'_{th}) \qquad (2)$$

Equation (2) reveals that the short circuit current is a consequence of the switch's intrinsic parameters, including its transconductance, threshold voltage, and the applied gate-emitter voltage. Reference [16] highlights that in a series structure, slight differences in the manufacturing process of switches, even those sharing the same part number, lead to variations in voltage distribution across them. The switch with lower transconductance (g_{fs}) will have a lower short-circuit current, leading it to operate in the active region with a higher collector-emitter voltage.

III. IGBT SCF BEHAVIOR IN ARM STRUCTURE

A. IGBT SCF behavior in Arm Structure Considering Identical devices

This paper focuses on a short-circuit scenario where the high-side IGBT (Q_H) operates normally, supplying power to the load. Meanwhile, the low-side IGBT (Q_L), shown in red, is erroneously triggered by an incorrect gate signal, resulting in a short-circuit fault (Figure 4). For simplicity, the effects of diode reverse recovery and load dynamics are neglected in the analysis.

Short-circuit events induce substantial current surges in both high-side and low-side IGBTs, potentially compromising device reliability. Understanding and characterizing this behavior is essential for improving the reliability of IGBT switches and converters. Figure 5 shows the arm switches' collector-emitter voltage and collector current waveforms, assuming identical gate drive conditions and IGBT characteristics. This study investigates the short-circuit fault in three stages: pre-fault ($t_0 < t < t_1$), transient ($t_1 < t < t_2$), and steady-state ($t_2 < t < t_3$). While the main focus is on steady-state behavior, the other stages are briefly reviewed to provide context.

Based on Fig.4, the IGBT currents can be expressed as follows:

$$I_L = I_H - I_{Load} = I_{Sc} \tag{3}$$

and

$$V_{QL} + V_{QH} = V_{Bus} \tag{4}$$

Where I_L and I_H denote the currents of Q_L and Q_H , respectively; I_{Load} indicates the load current, I_{Sc} is the short-circuit current, V_{QH} and V_{QL} are the collector-emitter voltages of Q_H and Q_L , respectively; V_{Bus} is the short-circuit bus voltage, and L_s is the stray inductance of the short-circuit path. As mentioned above, in the pre-fault stage, Q_H is conducting and operating in saturation region, while Q_L is off. In the transient stage, By applying an incorrect gate signal to Q_L , its voltage $V_{GE_{QL}}$ starts to increase when the gate-emitter voltage reaches the threshold voltage. Consequently, I_L and I_H are start to rise dramatically. An IGBT, which can be modeled as a Bipolar Junction Transistor (BJT) driven by a MOSFET [36], can be approximated using a BJT model, incorporating the early effect [37]. Thus :

$$\frac{dV_{CE}}{dI_{CE}} = R_{CE} \tag{5}$$

Combining (3) and (5)

$$I_L = I_H - I_{Load} \Rightarrow \frac{dI_L}{dt} = \frac{dI_H}{dt} \Rightarrow \tag{6}$$

$$d\left(\frac{V_{Q_L}}{R_{Q_L}}\right) = d\left(\frac{V_{Q_H}}{R_{Q_H}}\right) \Rightarrow d\left(\frac{V_{Q_H}}{V_{Q_L}}\right) = d\left(\frac{R_{Q_H}}{R_{Q_L}}\right)$$

By turning Q_L on, R_{QL} starts to decrease, but it is still much higher than R_{QH} . Thus, V_{QL} decreases, while V_{QH} increases. The rising V_{QH} will charge collector-gate parasitic capacitance (C_{CG}) of Q_H and furthermore charging gate-emitter (C_{GE}) parasitic capacitance, leading to an increase in $V_{GE_{QH}}$. This gate-emitter voltage rise cuases the short-circuit current to reach its peak. During this stage, the induced voltage on L_s mainly affects Q_L .

After the transient stage, IGBTs reach a steady-state condition in which voltages and currents stabilize. Considering equal parameters for the devices, as done in [31], it can be concluded that one device(Q_H) operates in the active region while the other (Q_L) operates in the saturation region. The voltage difference between the two devices is explained in Figure 6, which illustrates the IGBT's $I_{CE}-V_{CE}$ characteristics. Due to the inequality in the currents I_H and I_L , the high-side and low-side IGBTs experience different collector-emitter voltages. Furthermore, this voltage difference is directly proportional to the load current.

The voltage difference between IGBTs (ΔV_{CE}), assuming the IGBTs are identical, is calculated as [31]::

$$\Delta V_{CE} = -\frac{A_k (V_{GE} - V_{th})^2}{K_1 I_{Load}} \left[1 + \left(\frac{T_H}{T_L}\right)^{K_T}\right] + \frac{1}{K_1 I_{Load}} \{A_k^2 (V_{GE} - V_{th})^4 \left[1 + \left(\frac{T_H}{T_L}\right)^{K_T}\right]^2 + 2A_k (V_{GE} - V_{th})^2 \left[1 - \left(\frac{T_H}{T_L}\right)^{K_T}\right] (2 - 2K_0 - K_1 V_{Bus}) I_{Load} + (2 - 2K_0 - K_1 V_{Bus})^2 I_{Load}^2\}^{0.5} \quad (7)$$

Note that

$$\begin{cases} K_0 = \gamma \alpha_{T,N-Buffer} M \alpha_{T,N-Base0} \\ K_1 = \gamma \alpha_{T,N-Buffer} M \alpha_{T,N-Base1} \\ A_K = A K_a \\ \alpha_{T,N-Base}(V_{CE}) = \alpha_{T,N-Base1} V_{CE} + \alpha_{T,N-Base0} \end{cases} \quad (8)$$

, where A is the area factor, K_a is the trans-conductor of the MOS part, $\alpha_{T,N-Base}$ is the transport coefficient of the base region, M is the multiplication factor, γ is the injection efficiency of the collector-buffer junction, $\alpha_{T,N-Buffer}$ is the transport coefficient of the N buffer layer, T_H and T_L are the temperature of Q_H and Q_L, respectively; and K_T is the temperature correction factor. Equation (7) demonstrates the impact of the load current (I_{Load}) and the DC bus voltage on the voltage imbalance between IGBTs (ΔV_{CE}) in an arm structure during a short-circuit event. Specifically, it shows that the voltage difference (ΔV_{CE}) increases steadily as the load current rises.

B. IGBT SCF behavior in Arm Structure Considering Discrepancies in Devices Parameters

In more realistic operating conditions, IGBTs exhibit variations in their characteristics, such as non-identical variations in their gate-emitter voltages, gate-emitter threshold voltage (V_{TH}), and transconductance (g_{fs}). These variations can impact the voltage sharing(ΔV_{CE}), which describes voltage distribution among the IGBTs in the arm configuration. Consequently, equation (7), while accurate for ideal conditions, requires adjustments to reflect the behavior in these real-world scenarios accurately.

For better clarity, the voltage difference between the two IGBTs can be derived from equations (1) and (3) as follows:

$$\Delta V_{CE} = R_{oH} I_{Load} + I_{CE_L} (R_{oH} - R_{oL}) - R_{oH} g_{fs_H} (V_{GE_H} - V_{th_H}) + R_{oL} g_{fs_L} (V_{GE_L} - V_{th_L}) \quad (9)$$

Based on (9), voltage distribution across the IGBTs strongly depends on device parameters such as V_{TH} , and g_{fs} , as well as circuitry parameters, such as V_{GE} during SCF and the load current I_{Load} . Accordingly, the SCF energies are also different based on

$$\begin{cases} E_{SC-QH} = V_{QH} (I_{SC} + I_{Load}) t_{SC} \\ E_{SC-QL} = V_{QL} I_{SC} t_{SC} \end{cases} \quad (10)$$

Thus, the voltage and SCF energy distribution between the IGBTs is completely different. The next chapter will delve into the effects of discrepancies, exploring how they influence short-circuit voltage distribution and short-circuit current energy.

IV. Simulation Results

To more accurately represent real-world behavior under short-circuit conditions, the simulations incorporate intrinsic mismatches among IGBT devices. The most influential parameters in short-circuit behavior—identified based on Equation (1) and literature—are threshold voltage (V_{TH}), transconductance (g_{fs}), and gate-emitter voltage characteristics. Based on the information provided by IGBT manufacturers in their datasheets, the threshold voltage (V_{TH}) typically exhibits a variation range of approximately ±15%. Table 1 summarizes the V_{TH} variation for several commercial IGBT devices. datasheets usually report only a typical value for the device transconductance (g_{fs}), But in practice, (g_{fs}) can deviate substantially due to several issues such as junction temperature, manufacturing tolerance, device configuration, and gate-emitter voltage ranges. Furthermore, ageing phenomena—such as bond wire degradation, gate oxide wear-out, and increased on-state resistance—could slowly reduce the effective (g_{fs}) with time [16], [38]. Such considerations justify the ±15% variation range assumed for simulation purposes, to account for worst-case but realistic conditions.

A detailed simulation is conducted in PSPICE to clarify the influence of device discrepancies on their voltage distribution. In the simulation procedure, a double-test setup is considered for inductive load description, as reported in [34] and [38]. The specifications of the simulation case study are summarized in Table 2.
In all simulation results difference between devices' voltages during SCF is defined as

$$\Delta V_{CE} = V_{QH} - V_{QL} \tag{11}$$

A. Effect of devices' V_{TH} variation on their voltage distribution during SCF

Different simulations are conducted to assess the impact of devices' V_{TH} variation on their voltage during SCF. Figure 7-(a), presents the IGBTs voltages during SCF. As can be seen, voltage distribution of IGBTs depends on their V_{TH} value. Figure 7-(b), shows the summary of the SCF results in this scenario. Based on Figure 7-(b), ΔV_{CE} could be negative, zero, and considerably positive based on the discrepancy degree between the devices' V_{TH} values. When both devices are identical in terms of V_{TH} or Q_H exhibits a higher value of V_{TH} with respect Q_L , ΔV_{CE} has its maximum value since the SCF current of Q_H is more than the Q_L based on (2), which makes Q_H operate in the active region and Q_L in the saturation region.

B. Effect of devices g_{fs} variation on their voltage distribution during SCF

Figure 8-(a) provides the voltage of IGBTs during SCF when a difference in their transconductance value is considered. Regarding Figure 8-(a), Q_L could operate in a saturated region with a low voltage value during SCF when it has a lower value of g_{fs} and should operate in an active region with a higher value of g_{fs} . Figure 8-(b), shows the summary of SCF results when the devices' transconductance values vary. Considering Figure 8-(b), there is a decreasing profile for ΔV_{CE} when the transconductance value of Q_H grows. It can be explained that increasing the transconductance of Q_H enhances its current capability in the saturation region, so it can operate in the saturated region. However, in an identical case, Q_H is forced to operate in an active region with a high voltage value during SCF.

C. Effect of Load current on IGBTs voltage distribution during SCF

In this test condition, two IGBTs are considered to be completely identical, and the inductive load current changes from 0.5 A to 50 A. According to Figure 9-(a), the IGBT voltages are approximately balanced during SCF in light load conditions. In addition, in heavy loads, the high-side device is forced to operate in active region with a high voltage level. This fact is also reflected in Figure 9-(b), and it can be seen that ΔV_{CE} grows when the load current increases.

D. Effect of devices V_{GE} variation on their voltage distribution during SCF

As a circuitry parameter, the devices' gate-emitter voltages can change during SCF. This can be due to gate drive circuit and non-idealities that exist in the driver circuit parameters, which have been scrutinized in [39]. Figure 10-(a) presents the IGBTs collector-emitter voltages while the gate-emitter voltage of Q_H changes. Regarding Figure 10-(a), the Q_H voltage notably depends on its gate-emitter voltage. This voltage can determine the device operation region. At the low-value level of the device gate-emitter voltages, Q_H operates in the active region, and with high-values for gate-emitter voltage level, the device operates in the saturated region. Figure 10-(b) presents the detailed results of this test scenario for both Q_H and Q_L gate-emitter variation ranges.

From a general perspective, the short-circuit energy of the switches can vary, as the device carrying higher current also experiences higher voltage during the fault. According to the simulation results, this energy difference can increase or decrease depending on the intrinsic parameter mismatches. In an ideal condition where the switches have identical intrinsic parameters, the short-circuit energy may still differ by up to 30 times. Table 3. presents the short-circuit energy of the switches for a specific operating point in which both IGBTs are identical.

The results presented in this paper are based on a scenario in which the load current flows through the high-side switch while an incorrect gate signal is applied to the low-side switch. However, in the alternative case—where the load current passes through the low-side switch and an incorrect signal is applied to the high-side switch—a voltage redistribution still occurs. Furthermore, as in the presented scenario, variations in the intrinsic parameters of the devices also affect the behavior of this voltage redistribution. Figure 11 illustrates the alternative scenario, in which the load current flows through the low-side switch while an incorrect gate signal is applied to the high-side switch, similar to the previously discussed case. In this condition, the low-side switch, due to the higher current, operates in the active region, whereas the high-side switch remains in saturation. As a result, the short-circuit energy of the low-side switch becomes significantly larger than that of the high-side switch.

E. Discussion

Based on the existing literature, in the SCF for IGBTs in an arm configuration, the high-side device operates in the active region with a high level of voltage, and the lower device operates in the saturated region with negligible voltage. This results in two consequences that may be fatal in some circumstances:

1- The high-side device should bear an excessive level of SCF energy while having a higher voltage and current level than the lower device.
2- The high-side device will face a considerable overvoltage at the turning-off time due to the high SCF current value and the DC bus's parasitic inductance.

Based on the above-reported outcomes in previoues studies, [31] proposes to turn off the low-side device earlier to avoid high-voltage stress of the high-side device during SCF termination. However, the results provided in this section for a more realistic condition, considering differences in circuitry and device parameters, indicate that the above conclusions are incorrect on many occasions. Based on the results, the lower device can also enter the active region in SCF faults. Thus, the DC bus voltage shares between two IGBTs based on their intrinsic parameters. It has been shown that the low-side device can be in the active region while the high-side one operates in the saturation region. So, there can be conditions in which the SCF energies of the device are approximately the same. In addition, the [31] proposal may result in a fatal condition for the lower device since it bears a higher level of voltage with respect to the high-side device. Therefor, a turning-off strategy is mandatory to avoid dangerous conditions for both devices, which is lacking in the state of the art of the subject.

V. Experimental Results

To verify the simulation results, an experimental prototype is constructed. The photo of the experimental setup is presented in Figure 12. In addition, the specifications of the experimental prototype are provided in Table 4. According to the relationships (1) and (2), variations in intrinsic parameters such as threshold voltage and transconductance can be modeled by appropriately adjusting the gate-emitter voltage. A double test setup is fabricated with an inductor to realize the inductive load. In the second pulse, the load current reaches the desired value defined by the pulse width of the first pulse. The details of the double test setup are provided in [38]-[40] and ignored in this paper due to lack of space.

In the experiments, two parameters are adjusted, and the behavior of IGBTs during SCF is assessed. These two parameters are the devices gate-emitter voltage reflecting the deviation in the device V_{TH} value and the load current as a circuitry factor. Fig. 13-(a) presents the collector-emitter voltages of IGBTs during SCF when the gate-emitter voltage of the high-side device is set to 15 V and that of the low-side device is changed from 12 V to 15. 5 V. Fig. 13-(b) presents the results of a reverse condition where the low-side device gate-emitter voltage is fixed to 15 V and the high-side device gate-emitter voltage is adjusted from 12 V to 15.5 V. Fig. 13-(C) provides the summary of this SCF scenario. The results of Fig. 13 are coincide with the results of the simulation procedure. As anticipated, in conditions that the gate-emitter voltage of the high-side device is lower than that of the lower device, Q_H enters the active region and voltage redistribution occurs during SCF fault. However, in cases where the low-side device gate-emitter voltage is less than the high-side device one, the low-side device enters the active region, and voltage redistribution does not occur.

In the experiments, two parameters are adjusted and the behavior of IGBTs during SCF is assessed. These two parameters are devices gate-emitter voltage reflecting the deviation in the device V_{th} value and the load current as a circuitry factor. Figure 13-(a) presents the collector-emitter voltages of IGBTs during SCF when the gate-emitter voltage of the high-side device is set to 15 V and that of the low-side device is changed from 12 V to 15. 5 V. Figure 13-(b) presents the results of a reverse condition where the low-side device gate-emitter voltage is fixed to 15 V and the high-side device gate-emitter voltage is adjusted from 12 V to 15.5 V. Figure 13-(C) provides the summary of this SCF scenario. The results of Figure 13 are coincide with the results of the simulation procedure. As anticipated, in conditions that the gate-emitter voltage of the high-side device is lower than that of the lower device, Q_H enters the active region and voltage redistribution occurs during SCF fault. However, in cases where the low-side device gate-emitter voltage is less than the high-side device one, the low side device enters the active region and voltage redistribuion does not occur.

Figure 14-(a), presents the collector-emitter voltages of the devices during SCF in different load currents. Figure 14-(b) provides the results of these tests. Based on the results of Figure 14, in light loads, the voltage difference between two IGBTs is not notable during SCF. However, as expected in heavy loads, the high-side device enters into the active region and the a significant voltage/energy unbalance occurs for the IGBTs. This result is in line with thoes of the simulation and theoretical discussions. The negative voltage difference between the switches under light-load conditions in Figure 14 can be explained by the mismatch in intrinsic parameters. As previously discussed, at light loads, the voltage difference is expected to be small, but still positive. The observed negative polarity in the test case highlights the impact of intrinsic parameter variations among the switches.

VI. Conclusion

This paper describes the SCF behavior of IGBTs served in an arm configuration. In this study, practical assumptions are considered with respect to the extant literature consisting of internal and circuitry descripancies of IGBTs. Thus, modified results from the existing research articles are achieved. The main outcomes of this study are as

- voltage distribution of IGBTs in an arm configuration during SCF fault strictly depends on the differences in IGBTs' internal parameters, such as V_{th} and g_{fs}. So, the voltage redistribution of IGBTs reported in [31] may not occur in several circumstances.
- The circuit parameters, such as driver power supply voltage level and load current, also play an important role in voltage distributions over IGBTs during SCF.
- In light-load conditions, voltage redistribution which has been reported in [31], may not occur. However, the chance of voltage redistribution and considerable short circuit energy imbalance is high in heavy load.
- This uncertainty in voltage distribution among the IGBTs—and the resulting severe imbalance in short-circuit energy—can lead to device failure before the protection system is activated. Therefore, in addition to conventional short-circuit protection methods, an appropriate energy balancing method is required to equalize the short-circuit energy among the devices.

References

[1] Ariya, S. and Frede, B, "Monte Carlo Simulation With Incremental Damage for Reliability Assessment of Power Electronics," *IEEE Trans. Power Electron.*, vol. 36, no. 7, pp. 7366–7371, Jul. 2021, doi: 10.1109/TPEL.2020.3044438.

[2] Dhananjay, K., Rajesh Kumar,N., and Sushma,G., "Investigation of fault-tolerant capabilities of some recent multilevel inverter topologies," *Int. J. Electron.*, vol. 108, no. 11, pp. 1957–1976, Nov. 2021, doi: 10.1080/00207217.2020.1870752.

[3] Ui-Min, C,. Kyo-Beum Lee, Frede, B., and Kyo-Beum, L., "Study and Handling Methods of Power IGBT Module Failures in Power Electronic Converter Systems," *IEEE Trans. Power Electron.*, vol. 30, no. 5, pp. 2517–2533, May 2015, doi: 10.1109/TPEL.2014.2373390.

[4] Dawei, X., Li, R., Peter, T., et al., "Condition Monitoring Power Module Solder Fatigue Using Inverter Harmonic Identification," *IEEE Trans. Power Electron.*, vol. 27, no. 1, pp. 235–247, Jan. 2012, doi: 10.1109/TPEL.2011.2160988.

[5] Jayakrishnan, H., Giampaolo, B., Giovanni, M., *et al.*, "Failure Modes and Reliability Oriented System Design for Aerospace Power Electronic Converters," *IEEE Open J. Ind. Electron. Soc.*, vol. 2, pp. 53–64, 2021, doi: 10.1109/OJIES.2020.3047201.

[6] Azra, M., Ahteshamul, H., and Kurukuru, V. S., "Fault Tolerant Inverter for Grid Connected Photovoltaic System," in *2022 IEEE International Conference on Power Electronics, Smart Grid, and Renewable Energy (PESGRE)*, Jan. 2022, pp. 1–6. doi: 10.1109/PESGRE52268.2022.9715825.

[7] Yantao, S. and Bingsen, W., "Survey on Reliability of Power Electronic Systems," *IEEE Trans. Power Electron.*, vol. 28, no. 1, pp. 591–604, Jan. 2013, doi: 10.1109/TPEL.2012.2192503.

[8] Md, Abul, M., "Penalty for Fuel Economy— System Level Perspectives on the Reliability of Hybrid Electric Vehicles During Normal and Graceful Degradation Operation," *IEEE Syst. J.*, vol. 2, no. 4, pp. 476–483, Dec. 2008, doi: 10.1109/JSYST.2008.2005714.

[9] Alan, R., Miroslav, B., Aleksandar, P., et al., "Development of a Methodology for Improving Photovoltaic Inverter Reliability," *IEEE Trans. Ind. Electron.*, vol. 55, no. 7, pp. 2581–2592, Jul. 2008, doi: 10.1109/TIE.2008.924017.

[10] Victor, A., Jose de Jesus, R., Jose Hugo, B., et al., "Review of fault detection techniques in power converters: Fault analysis and diagnostic methodologies," Measurement, vol. 234, p. 114864, Jul. 2024, doi: 10.1016/j.measurement.2024.114864.

[11] Marco, di B., Alessandro, L., Luca, S., et al., "Reliability and Real-Time Failure Protection of the Three-Phase Five-Level E-Type Converter," *IEEE Trans. Ind. Appl.*, vol. 56, no. 6, pp. 6630–6641, Nov. 2020, doi: 10.1109/TIA.2020.3019358.

[12] Sadegh, M., "An Online Condition Monitoring Method for Series-Connected IGBTs to Avoid Cascading Failure," *IEEE Trans. Ind. Electron.*, pp. 1–9, 2022, doi: 10.1109/TIE.2022.3219087.

[13] Saeed, P., Peter, P., and Frede, B., "An Overview on the Reliability of Modern Power Electronic Based Power Systems," *IEEE Open J. Power Electron.*, vol. 1, pp. 34–50, 2020, doi: 10.1109/OJPEL.2020.2973926.

[14] Sadegh, M., Mostafa, Z., and Shahriyar, K., "A Voltage Balancing Scheme for Series IGBTs to Increase Their Expected Lifetime in Pulsed Load Applications," *IEEE J. Emerg. Sel. Top. Power Electron.*, vol. 9, no. 1, pp. 461–471, Feb. 2021, doi: 10.1109/JESTPE.2019.2958357.

[15] Noriyuki, I., and Thomas, L., "IGBT History, State-of-the-Art, and Future Prospects," *IEEE Trans. Electron Devices*, vol. 64, no. 3, pp. 741–752, Mar. 2017, doi: 10.1109/TED.2017.2654599.

[16] Sadegh, M., Mostafa, Z., and Shahriyar, K., "A Series Stacked IGBT Switch With Robustness Against Short-Circuit Fault for Pulsed Power Applications," *IEEE Trans. Power Electron.*, vol. 33, no. 5, pp. 3779–3790, May 2018, doi: 10.1109/TPEL.2017.2712705.

[17] Rahul, S. Ch., Jamie, C., and Laszlo, K., "A discussion on IGBT short-circuit behavior and fault protection schemes," *IEEE Trans. Ind. Appl.*, vol. 31, no. 2, pp. 256–263, Mar. 1995, doi: 10.1109/28.370271.

[18] Sadegh, M., Javad, N., and Kamyar, M., "Reliability Enhancement of Power IGBTs under Short-Circuit Fault Condition Using Short-Circuit Current Limiting-Based Technique," *Energies*, vol. 14, no. 21, Art. no. 21, Jan. 2021, doi: 10.3390/en14217397.

[19] Sadegh, M., Mostafa, Z., and Shahriyar, K., "A Voltage Balancing Method for Series-Connected IGBTs Operating as A Fault Current Limiter in High Voltage DC Power Supplies," *IEEE Trans. Ind. Electron.*, pp. 1–1, 2020, doi: 10.1109/TIE.2020.3009606.

[20] Sadegh, M., Mostafa, Z., and Shahriyar, K., "A Series Stacked IGBT Switch to Be Used as a Fault Current Limiter in HV High Power Supplies," *IEEE J. Emerg. Sel. Top. Power Electron.*, pp. 1–1, 2021, doi: 10.1109/JESTPE.2021.3061093.

[21] Kummara Venkat Guru, R., Kamran, Z., Anand, M., *et al.*, "A Comprehensive Review of DC–DC Converter Topologies and Modulation Strategies with Recent Advances in Solar Photovoltaic Systems," *Electronics*, vol. 9, no. 1, Art. no. 1, Jan. 2020, doi: 10.3390/electronics9010031.

[22] Mojtaba, F., Yam, P. S., Saman, A. Gorji., et al., "Step-Up DC–DC Converters: A Comprehensive Review of Voltage-Boosting Techniques, Topologies, and Applications," *IEEE Trans. Power Electron.*, vol. 32, no. 12, pp. 9143–9178, Dec. 2017, doi: 10.1109/TPEL.2017.2652318.

[23] Nami; Liang; Dijkhuizen Alireza, N., Jiaqi, L., Frans, D., et al., "Modular Multilevel Converters for HVDC Applications: Review on Converter Cells and Functionalities," *IEEE Trans. Power Electron.*, vol. 30, no. 1, pp. 18–36, Jan. 2015, doi: 10.1109/TPEL.2014.2327641.

[24] He, D., Ichiro, O., Shuhei, M., et al., "Investigation of the Parasitic Inductance Influence on the Short-Circuit Behaviour of High Voltage IGBTs," in 2023 IEEE Applied Power Electronics Conference and Exposition (APEC), Mar. 2023, pp. 2451–2455. doi: 10.1109/APEC43580.2023.10131377.

[25] Jan, F., Sebastian, K., Hans-Guenter, E., "IGBT and Diode Behavior During Short-Circuit Type 3," *IEEE Trans. Electron Devices*, vol. 62, no. 11, pp. 3786–3791, Nov. 2015, doi: 10.1109/TED.2015.2477324.

[26] Thomas, B., Riteshkumar, B., Josef, L., et al., "Dynamic self-clamping at short-circuit turn-off of high-voltage IGBTs," in *2013 25th International Symposium on Power Semiconductor Devices & IC's (ISPSD)*, May 2013, pp. 277–280. doi: 10.1109/ISPSD.2013.6694440.
[27] Xing, L., Jens, K., Clemens, H., et al., "The Influence of the Gate Driver and Common-Source Inductance on the Short-Circuit Behavior of IGBT Modules and Protection," *IEEE Trans. Power Electron.*, vol. 35, no. 10, pp. 10789–10798, Oct. 2020, doi: 10.1109/TPEL.2020.2981427.
[28] Xing, L. and Thomas, B., "Investigation of the Gate Voltage Overshoot of IGBTs Under Short Circuit Type II Condition," IEEE Trans. Electron Devices, vol. 70, no. 4, pp. 1763–1768, Apr. 2023, doi: 10.1109/TED.2023.3247371.
[29] Jan, F., Hans-Guenter, E., and Sebastian, K., "Short-circuit behavior of series-connected high-voltage IGBTs," in *2016 18th European Conference on Power Electronics and Applications (EPE'16 ECCE Europe)*, Sep. 2016, pp. 1–10. doi: 10.1109/EPE.2016.7695445.
[30] Matthias, S. and Georg, K., "Current sharing between parallel IGBTs in power modules during short circuit with unsymmetrically connected load," in *2016 18th European Conference on Power Electronics and Applications (EPE'16 ECCE Europe)*, Sep. 2016, pp. 1–9. doi: 10.1109/EPE.2016.7695365.
[31] Yixuan, Y., Yilin, W., Xuebao, L., *et al.*, "Short-Circuit Behavior and Voltage Redistribution of IGBTs in Bridge Structures," *IEEE Trans. Power Electron.*, vol. 38, no. 3, pp. 3824–3833, Mar. 2023, doi: 10.1109/TPEL.2022.3208592.
[32] Bin, L. and Santosh, K. S., "A Literature Review of IGBT Fault Diagnostic and Protection Methods for Power Inverters," *IEEE Trans. Ind. Appl.*, vol. 45, no. 5, pp. 1770–1777, Sep. 2009, doi: 10.1109/TIA.2009.2027535.
[33] Amir, A. R. and Sadegh, M., "Interrelation of Gate Resistance and Emitter/Source Inductance Impact on Inductive Load Phase-Leg Crosstalk," IEEE J. Emerg. Sel. Top. Ind. Electron., vol. 6, no. 1, pp. 415–424, Jan. 2025, doi: 10.1109/JESTIE.2024.3476274.
[34] Amir, A. R. and Sadegh, M., "Interrelation of Gate Resistance and Emitter/Source Inductance Impact on Inductive Load Phase-Leg Crosstalk," *IEEE J. Emerg. Sel. Top. Ind. Electron.*, pp. 1–10, 2024, doi: 10.1109/JESTIE.2024.3476274.
[35] Anis, A., Bruno, A., and Hervé, M., "Transient temperature measurements and modeling of IGBT's under short circuit," IEEE Trans. Power Electron., vol. 13, no. 1, pp. 12–25, Jan. 1998, doi: 10.1109/63.654955.
[36] Alicia, T., Yosuke, M., Mitiko, M.M., et al., "HiSIM_IGBT2: Modeling of the Dynamically Varying Balance Between MOSFET and BJT Contributions During Switching Operations," IEEE Trans. Electron Devices, vol. 66, no. 8, pp. 3265–3272, Aug. 2019, doi: 10.1109/TED.2019.2919799.
[37] Bryan, L. H., "Modeling the Early Effect in Bipolar Transistors," IEEE J. Solid-State Circuits, vol. 18, no. 1, pp. 139–140, Feb. 1983, doi: 10.1109/JSSC.1983.1051910.
[38] Mojtaba, J., Sadegh, M., Javad, N., et al., "Real-Time Degradation Level Assessment of IGBT Gate Oxide Layer Using Turn-Off Delay Time," *IEEE Trans. Power Electron.*, vol. 38, no. 12, pp. 16153–16164, Dec. 2023, doi: 10.1109/TPEL.2023.3319379.
[39] Sadegh, M., "A Gate Driving Strategy for the Series-Connected IGBTs to Improve the Resilience Against IGBTs Short-Circuit Failures," *IEEE Trans. Ind. Electron.*, vol. 69, no. 10, pp. 9961–9971, Oct. 2022, doi: 10.1109/TIE.2021.3137594.
[40] Allahyar, M., Sadegh, M., and Khatereh, A., "An Online Condition Monitoring Method for IGBT Gate Oxide Degradation Based on the Gate Current in Miller Plateau," *IEEE Trans. Ind. Electron.*, pp. 1–9, 2022, doi: 10.1109/TIE.2022.3210581.

List of figures

List of tables

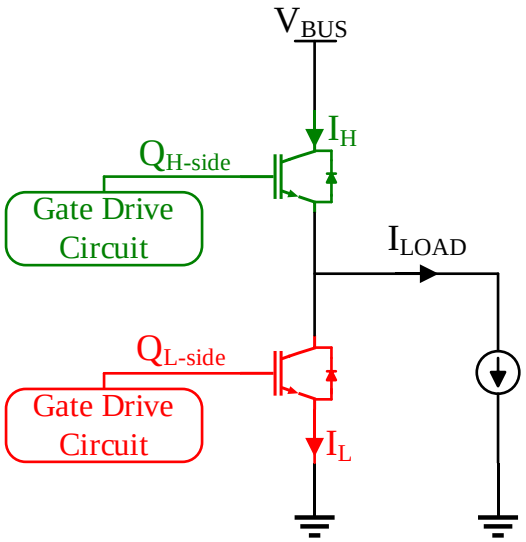

Figure 1: Arm configuration circuit.

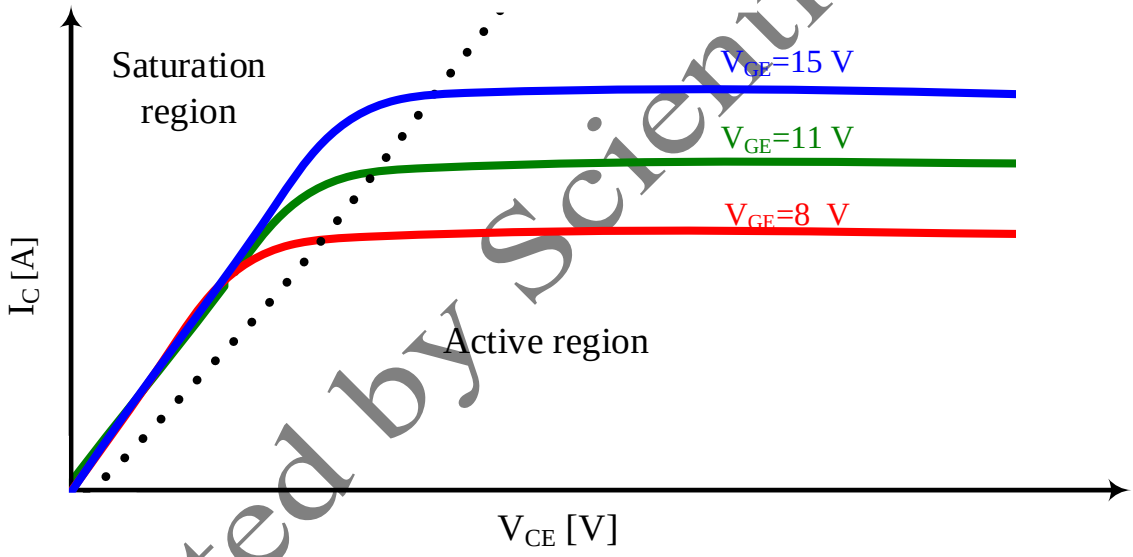

Figure 2: IGBT transfer characteristics.

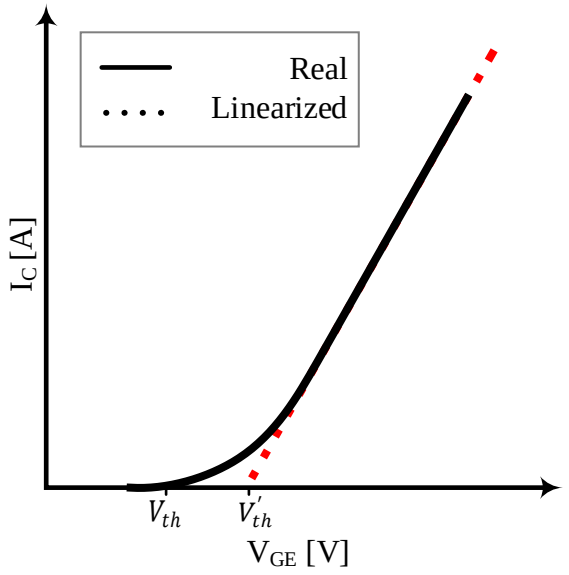

Figure 3: IGBT real and linearized IC-VGE characteristics.

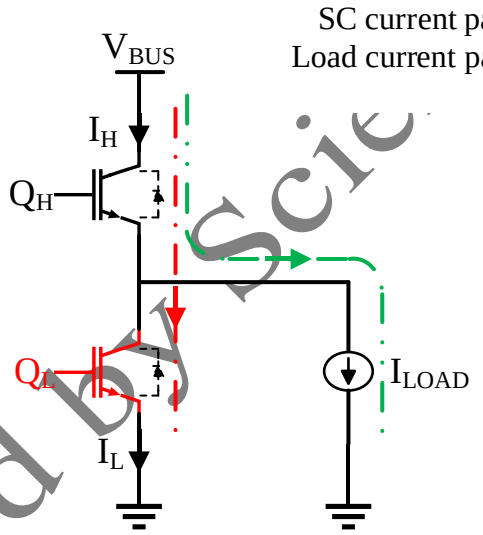

Figure 4: Simplified circuit model for analyzing short-circuit fault due to malfunction of gate drive circuitry.

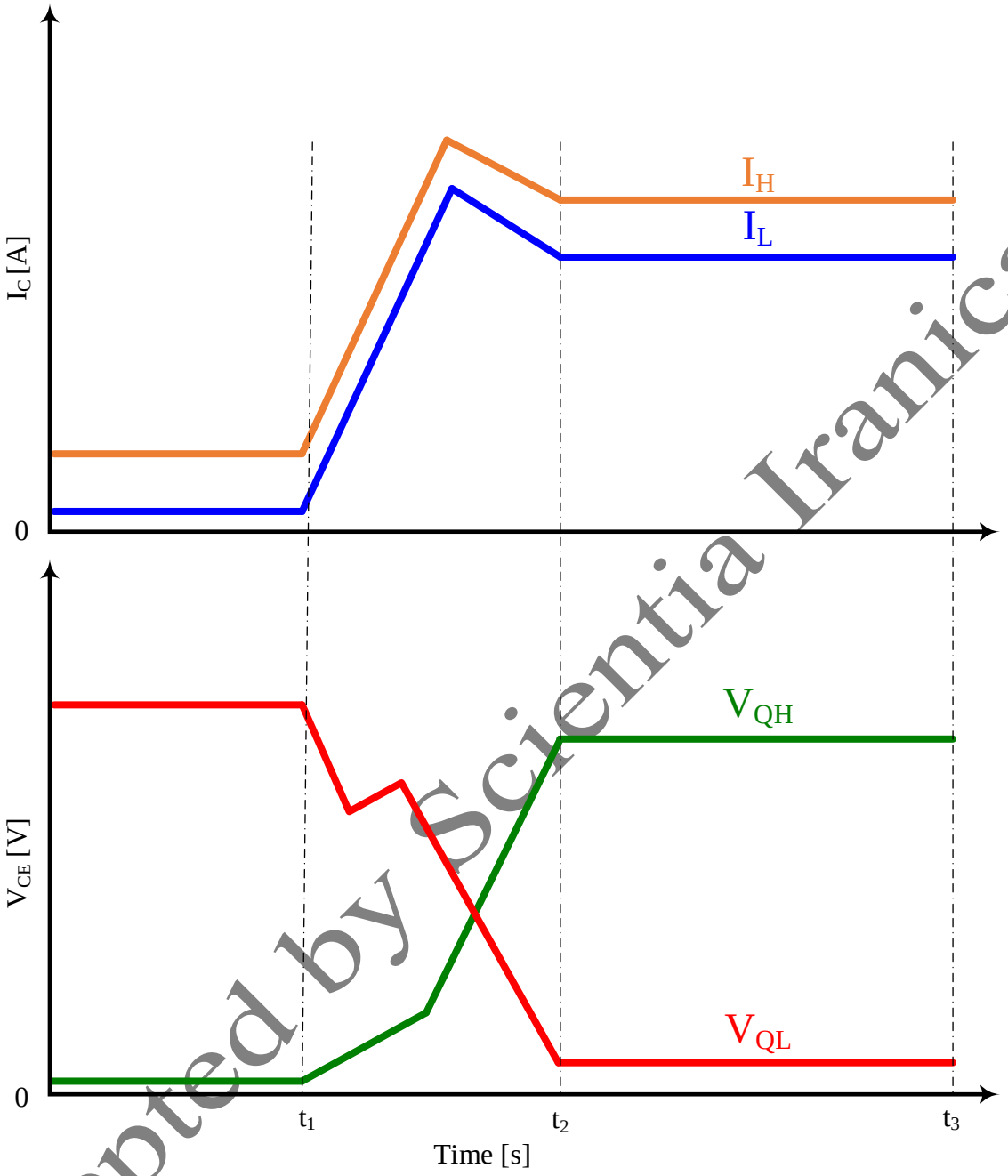

Figure 5: IGBT Collector-Emitter Voltage and Collector Current Waveforms During Different Stages of a Short-Circuit Fault.

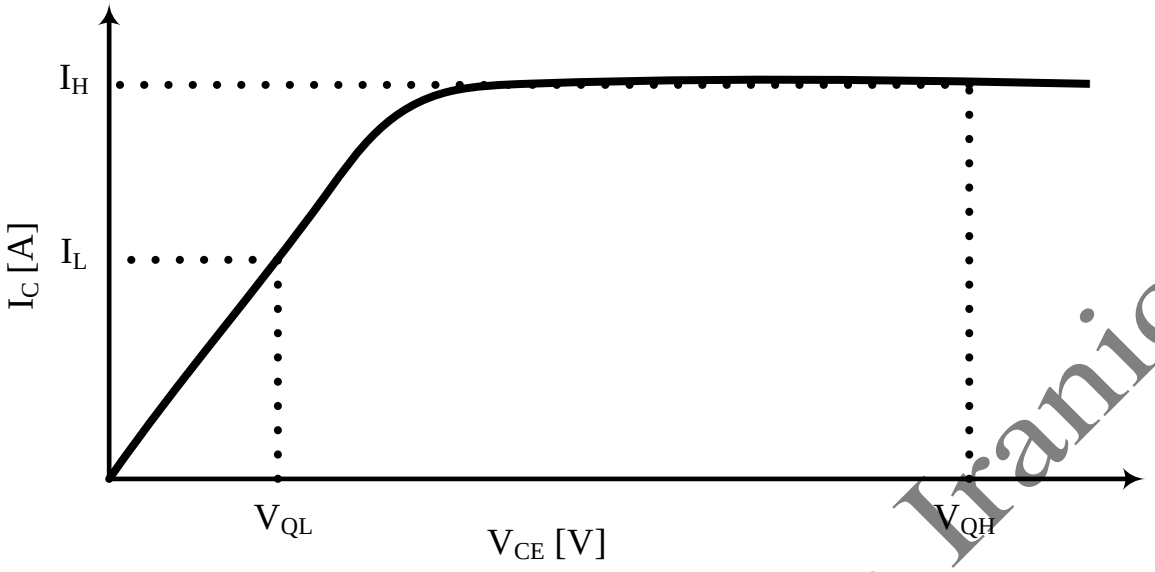

Figure 6: IGBT's IC-VCE characteristics in steady state stage with equal gate-emitter voltages and identical switches.

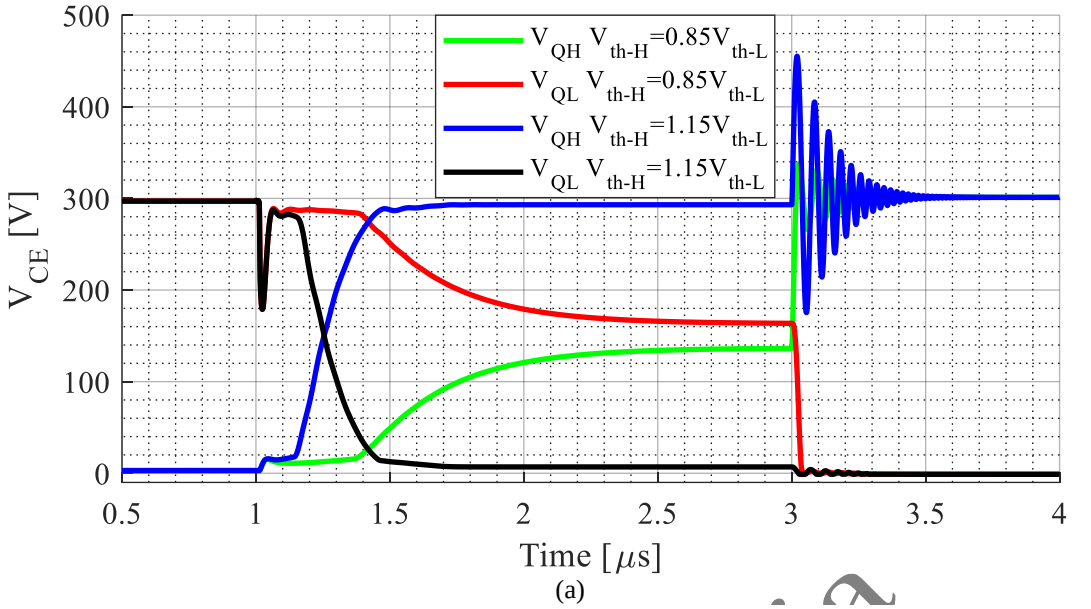

(a)

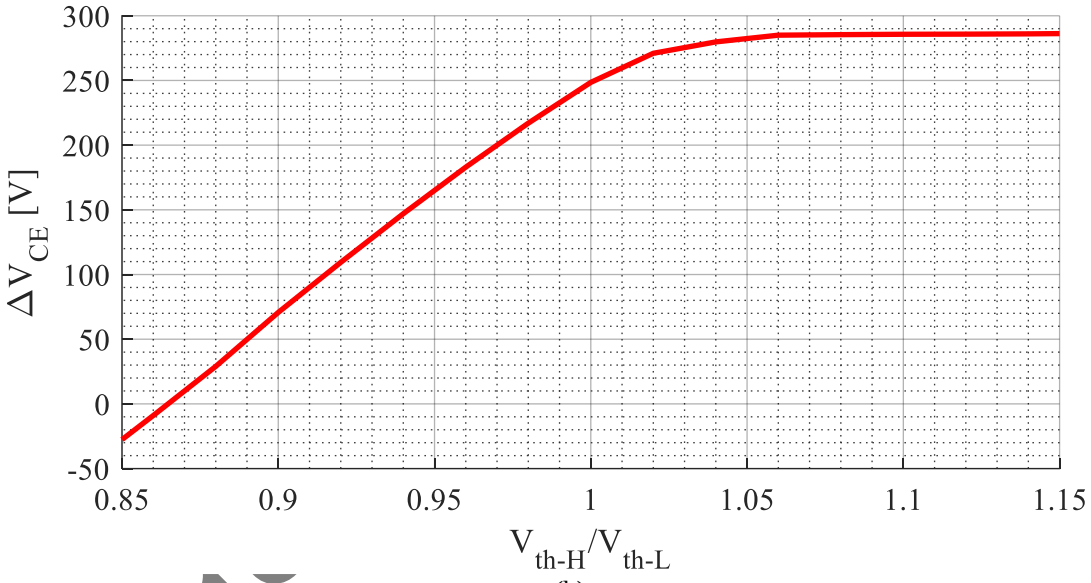

(b)

Figure 7: The simulated voltage waveforms of the devices during short circuit fault when discrepancies exist in their threshold voltages (a), the difference in the devices voltages in steady state short circuit time interval while threshold voltages change.

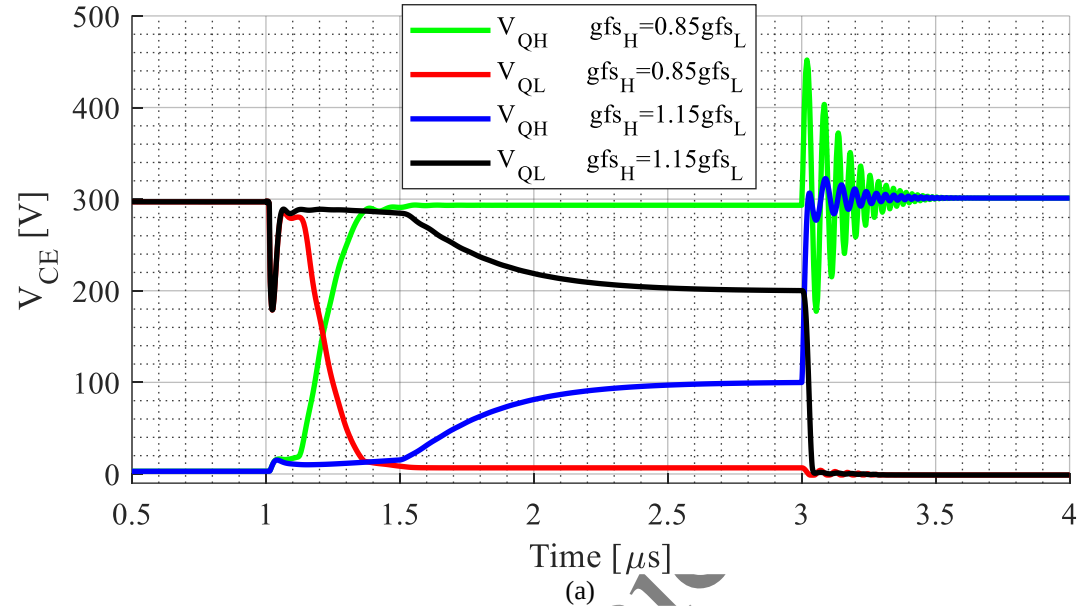

(a)

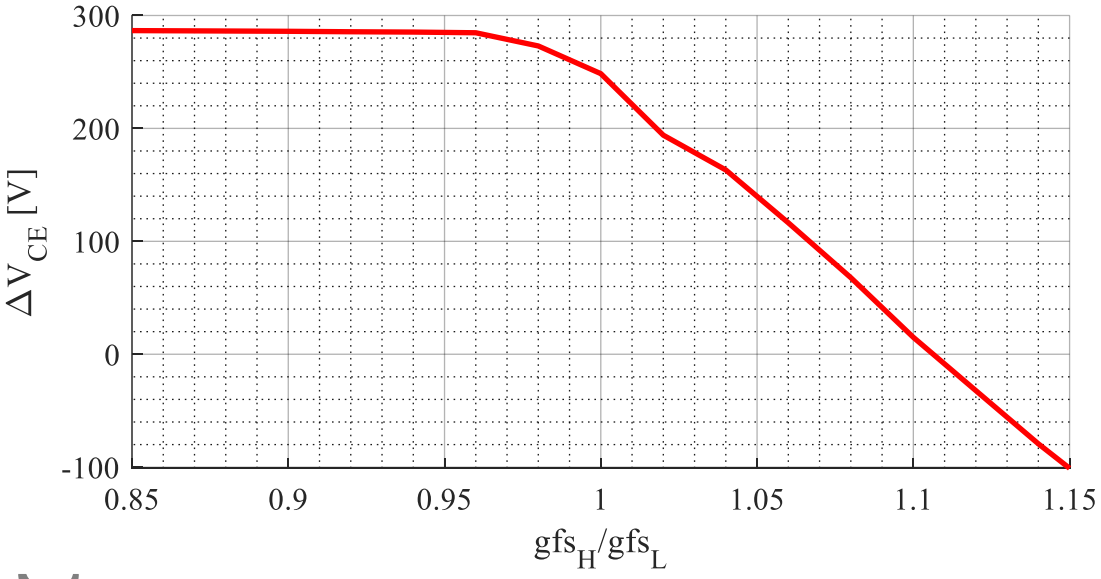

(b)

Figure 8: The simulated voltage waveforms of the devices during short circuit fault when discrepancies exist in their transconductance (a), the difference in the devices voltages in steady state short circuit time interval while transconductance values change(b).

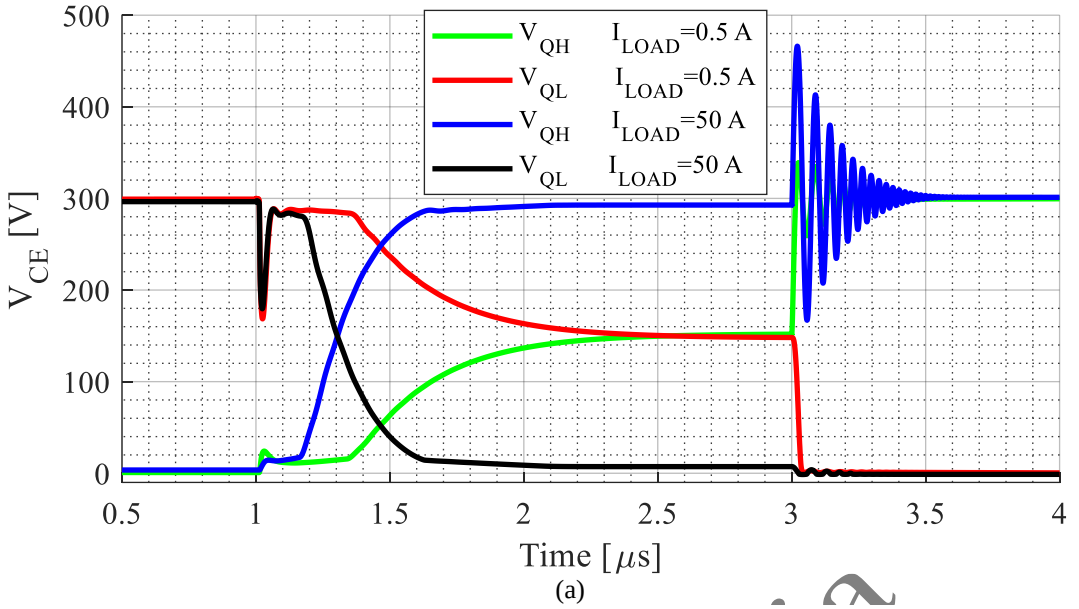

(a)

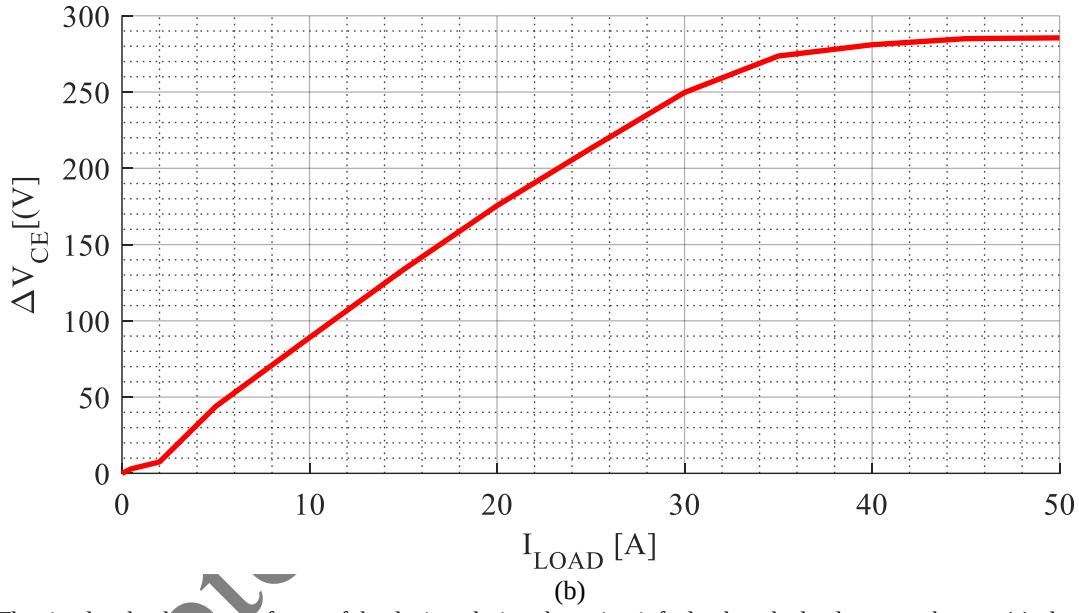

(b)

Figure 9: The simulated voltage waveforms of the devices during short circuit fault when the load current changes (a), the difference in the devices voltages in steady state short circuit time interval while load current changes(b).

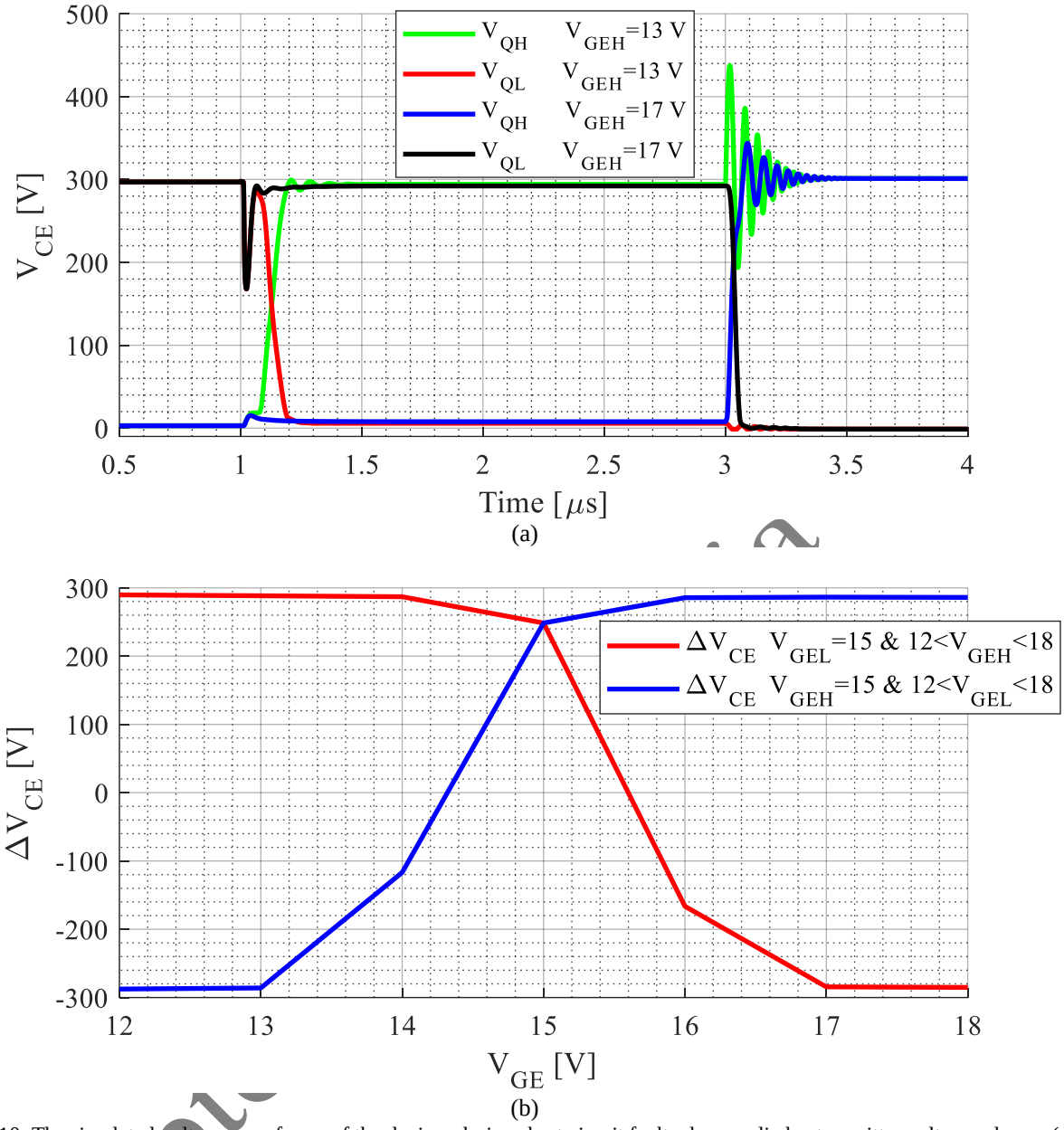

Figure 10: The simulated voltage waveforms of the devices during short circuit fault when applied gate-emitter voltages change (a), the difference in the devices voltages in steady state short circuit time interval while the devices gate-emitter voltages changes (b).

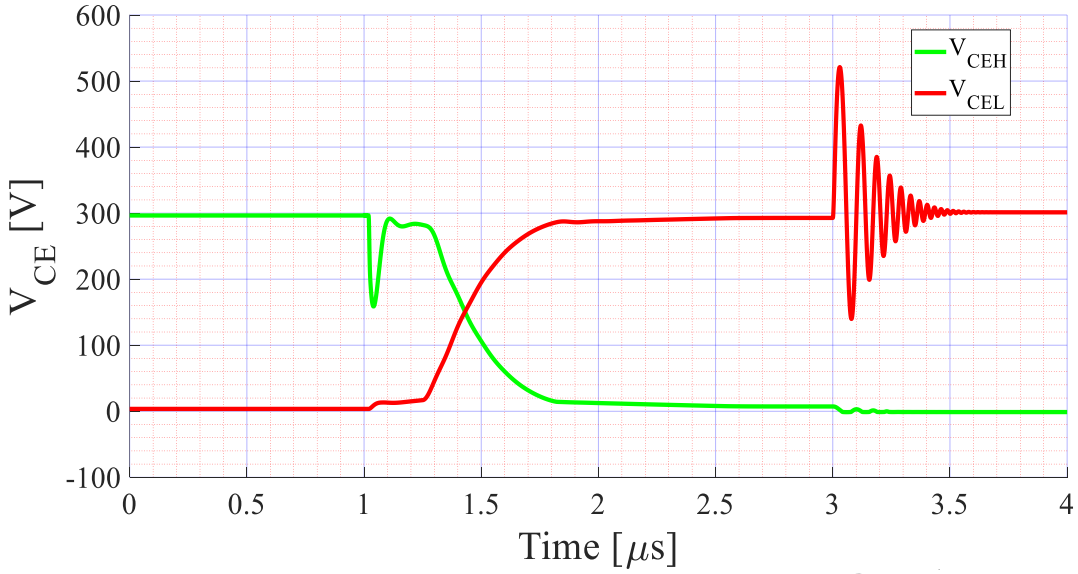

Figure 11: The simulated voltage waveforms of the devices during short circuit fault when load current flow through low-side IGBT and incorrect gate signal applied to high-side IGBT.

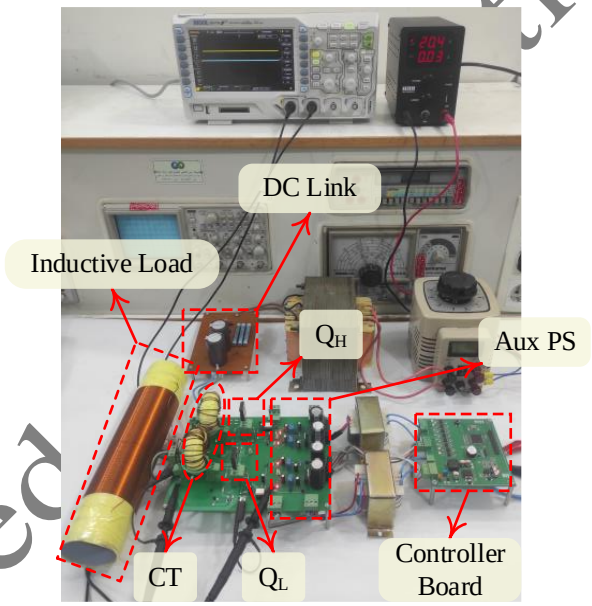

Figure 12: The photo of the experimental setup for conducting short circuit faults for IGBTs in an arm configuration.

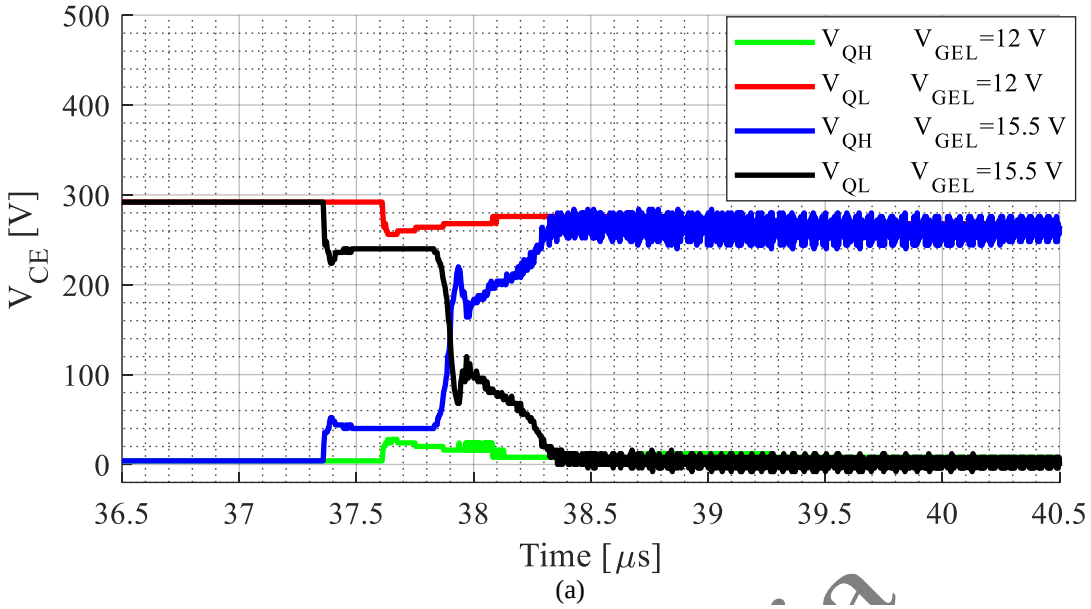
500
400
300
200
100
0
V_{CE} [V]
36.5
37
37.5
38
38.5
39
39.5
40
40.5
Time [μs]
V_{QH} V_{GEL}=12 V
V_{QL} V_{GEL}=12 V
V_{QH} V_{GEL}=15.5 V
V_{QL} V_{GEL}=15.5 V

(a)

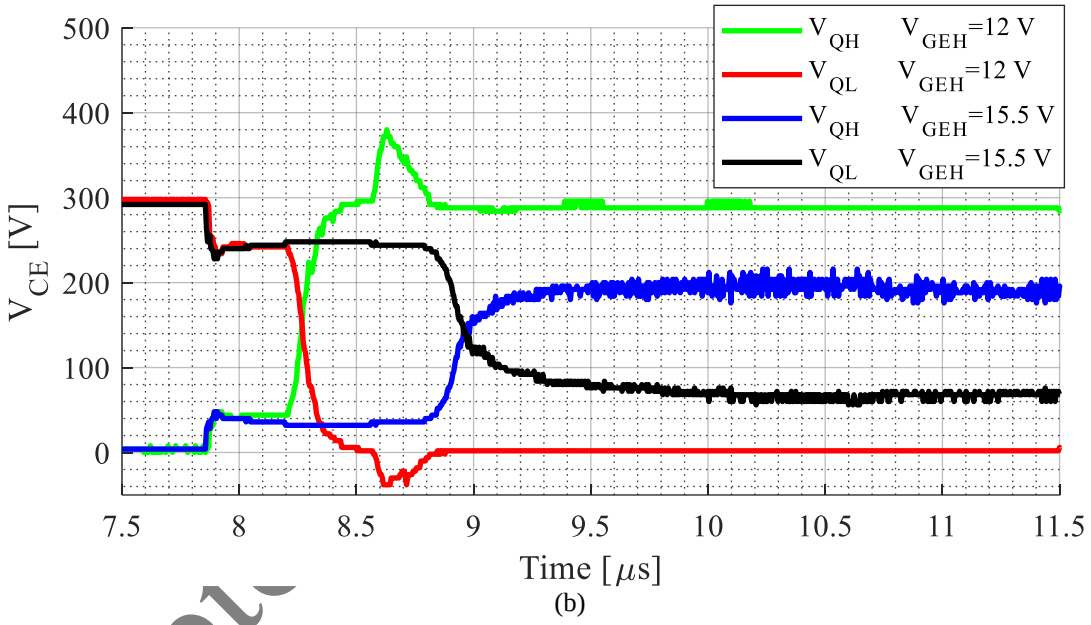
500
400
300
200
100
0
V_{CE} [V]
7.5
8
8.5
9
9.5
10
10.5
11
11.5
Time [μs]
V_{QH} V_{GEH}=12 V
V_{QL} V_{GEH}=12 V
V_{QH} V_{GEH}=15.5 V
V_{QL} V_{GEH}=15.5 V

(b)

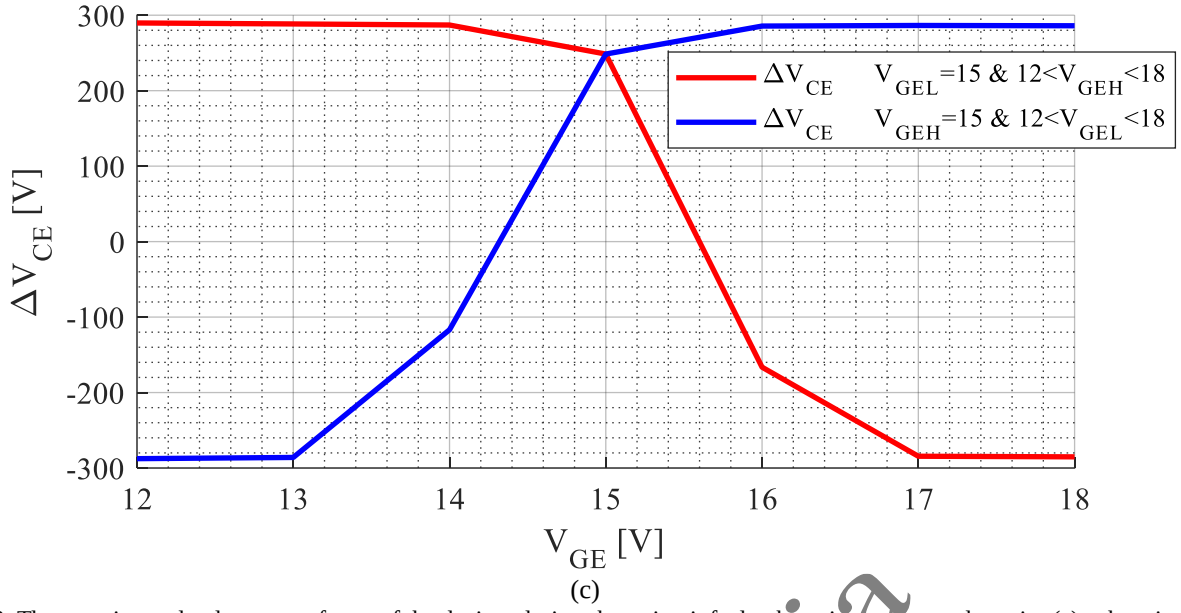

(c)

Figure 13: The experimental voltage waveforms of the devices during short circuit fault when is constant and varies (a), when is constant and varies (b) the difference in the devices voltages in steady state short circuit time interval while devices gate-emitter voltages changes (c).

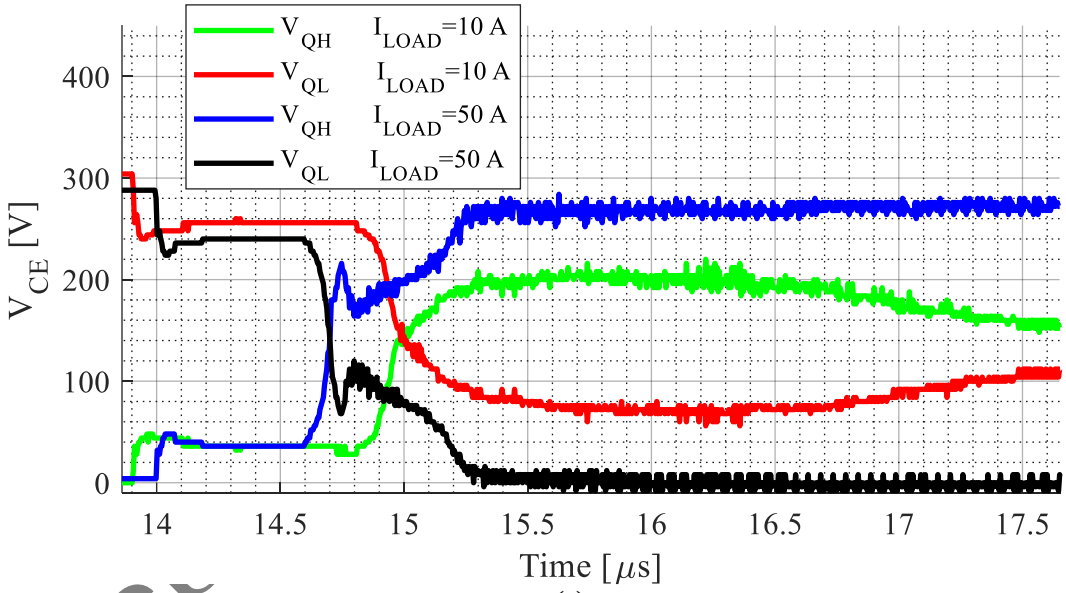

(a)

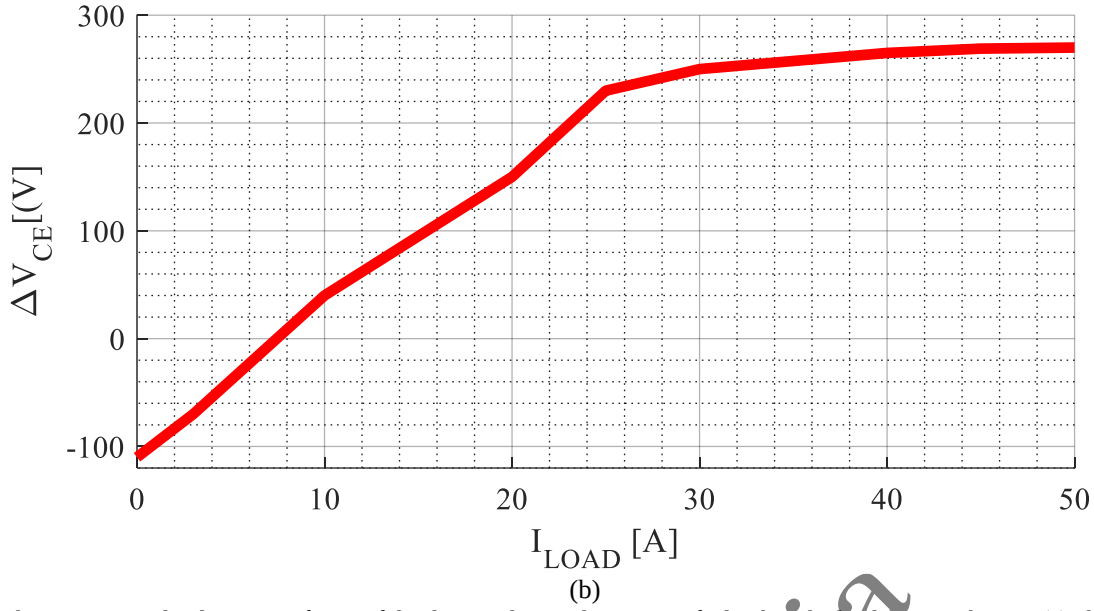

(b)

Figure 14: The experimental voltage waveforms of the devices during short circuit fault when the load current changes (a), the difference in the devices voltages in steady state short circuit time interval while devices the load current changes (b).

Table 1: Threshold voltage variation range for several commercial IGBT devices.

IGBT Part Number	$+\Delta V_{TH}$	$-\Delta V_{TH}$
AIKQ100N60CT	+16.3 %	-16.3 %
IKW30N60H3	+11.7 %	-19.6 %
STGWA30IH160DF2	+16.6 %	-16.6 %

Table 2: The specifications of PSPICE simulation.

Parameter	Value
V_{Bus}	300 V
I_{Load}	0.5 A~ 50 A
Devices part number	IXGH30N60
Load inductance	2 *mH*
Device V_{TH} variation range	+-15 %
Device g_{fs} variation range	+-15 %
Device gate-emitter voltage during SCF	15 V +-15 %
DC bus parasitic inductance	100 *nH*
Short-Circuit Starting Time in Figure 7 to Figure 10	1 μs
Short-Circuit Termination Time in Figure 7 to Figure 10	3 μs

Table 3: The short-circuit energy of IGBTs.

	E_{scH}	E_{scL}
SCF Energy	≈320 mJ	≈9.2 mJ

Table 4: The specifications of the experimental prototype.

Parameter	Value
V_{Bus}	100 V~300 V
I_{Load}	0.5 A~ 50 A
Devices part number	IXGH30N60
IGBT driver part number	HCPL3120
SCF frequency	1 *Hz*
Load inductance	2 *mH*
Device V_{TH} variation range	+-15 %
Device g_{fs} variation range	+-15 %
Device gate-emitter voltage during SCF	15 V +-15 %
DC bus parasitic inductance	100 *nH*
DC bus capacitance	2 *mF*

Biographies

Naser Mohammad-Bagheri Bafghi

Naser Mohammad-Bagheri Bafghi received the B.Sc. degree in electrical engineering from the Isfahan University of Technology, Iran, in 2022, and the M. Sc. Degree from K. N. Toosi University of Technology, Tehran, Iran, in the field of power electronics, in 2025. His research interests include condition monitoring, reliability in Power electronics Converters , resonant converters, and Grid-Tied solar inverters.

Sadegh Mohsenzade

Sadegh Mohsenzade (Member, IEEE) received the M.Sc. and Ph.D. degrees in power electronics from the Sharif University of Technology, Tehran, Iran, in 2016 and 2019, respectively. He currently is an Assistant Professor with the K. N. Toosi University of Technology, Tehran, Iran, in the field of power electronics. His research interests include high-voltage pulsed power supplies, resonant converters, condition monitoring, and reliability in power electronic converters.